15th Nordic Laser Materials Processing Conference

Laser welding process – a review of keyhole welding modelling

Josefine Svenungsson[a]*, Isabelle Choquet[a], Alexander F. H. Kaplan[b]

[a]*University West, Department of Engineering Science, 461 32 Trollhättan, Sweden*
[b]*Luleå University of Technology, Department of Engineering Science and Mathematics, 971 87 Luleå, Sweden*

Abstract

Laser welding is used in several industrial applications. It can be distinguished between conduction mode and keyhole mode welding, between pulsed wave and cw laser welding and between CO_2-lasers with a wavelength of 10 µm and various laser types of about 1 µm wavelength. A deeper understanding of laser welding allows improving weld quality, process control and process efficiency. It requires a complementary combination of precise modelling and experimental investigations. The here presented review focuses on modelling of laser keyhole welding, for both wavelength regimes. First, the fundamentals of the laser welding process and its physics such as beam propagation, keyhole formation and melt pool dynamics are addressed. The main approaches for modeling energy transfer from laser beam to keyhole surface as well as fluid flow in the material are then discussed. The most relevant publications are systematically structured, particularly categorized with regard to the respective physical phenomena addressed. Finally some open questions are underlined.

Selection and blind-review under responsibility of Lappeenranta University of Technology.

Keywords: keyhole, liquid flow, vapour flow, melting, vaporization, plasma, Fresnel absorptions, inverse Bremmstralhung absorption, modeling.

1. Introduction

Laser welding is a rather recent technology compared to conventional arc welding methods. Its main advantages are the larger welding speed, the low energy input into the metal, the narrow bead produced, and the small heat affected zone. Its most common imperfections are humping, porosity and spatter. Some imperfections may also result from the small beam diameter. Without filler material, the pieces to be welded need to be closely adjusted. Inaccurate beam positioning can then result in lack of fusion, concave root surfaces, and sagged welds. The high cooling rates may also lead to pore formation in very deep welds with insufficient degassing. Experimental and modelling investigations can supplement each other to deeper understand this process, the causes of defects and further improve weld quality.

* Corresponding author. *E-mail address:* josefine.svenungsson@hv.se

Selection and blind-review under responsibility of Lappeenranta University of Technology.

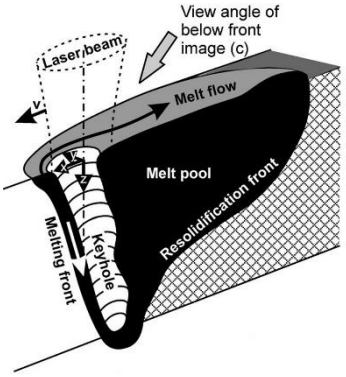

Fig. 1. Sketch of laser beam, keyhole and melt pool, Kaplan (2012).

Laser welding requires large power density ranging from about 5×10^4 to 10^7 W/cm^2. This power can be provided by CO_2 gas laser (with a wavelength of the order of 10 μm) as well as solid state lasers such as Nd:YAG - rod, Yb:YAG - disk and Yb:glass - fiber (with wavelengths of the order of 1 μm).

For a workpiece made of steel for instance and a CO_2 laser beam intensity below about 10^5 W/cm^2, the laser light is strongly reflected by the material and less than 30% of the beam energy is absorbed at the workpiece surface (via direct Fresnel absorption). This case (called conduction laser welding) results in shallow weld penetration characterized by weld bead with depth to width ratio of the order of one.

Transition to keyhole laser welding occurs at about 10^6 W/cm^2 due to the enhancement of metal vaporization. The intense vaporization distinguishes keyhole laser welding from other conventional joining methods. It causes a large increase in vapour pressure (recoil pressure) that drills a depression in the melted metal, forming a long and narrow cavity or keyhole. The laser beam can then penetrate deeper into the metal through the cavity and be refracted and damped while traveling through the vapour. As the beam rays reach the keyhole surface, beam energy is partially absorbed on the surface and partially reflected towards a new point of interaction. This succession of absorption/reflection (or multiple reflection Fresnel absorption) increases the overall energy absorption (up to 90% in the present example). In that case the weld bead is much deeper than for conduction laser welding; its depth to width ratio can reach the order of 100. Figure 1 illustrates the laser beam above the keyhole, the melt flowing around the keyhole from the melting front, and the solidification front of the melt pool.

The keyhole cavity is filled with metal vapour that partly absorbs the incoming laser light. The charged particles present in the vapour can gain kinetic energy from the beam photons via inverse Bremsstrahlung absorption (iB-absorption). When the gain is significant it results in beam damping, further ionization of the metal vapour (plasma) by the highly energetic electrons, increase of the plasma temperature, and in turn increase of the iB-absorption coefficient as long as the plasma temperature does not exceed some critical value, see Zhou et al. (2006). The plasma has then a positive role: it can protect the keyhole cavity from cooling by the surrounding atmosphere and plasma radiation can strengthen vaporization at the keyhole surface. Above the critical temperature damping becomes dominant and vaporization vanishes.

The metal vapour can also agglomerate into larger nm-size particles forming fumes. Particles of size comparable to or larger than the beam wavelength attenuate the laser power through Mie-scattering while much smaller particles attenuate it through Rayleigh scattering.

The metal vapour flows out of the cavity forming a plume while being replaced by newly evaporated material. The plume can also participate to beam damping, Mościcki et al. (2006). As the absorption and the scattering coefficients are temperature dependent, they are also coupled to the plasma properties and temperature field. Absorption depends also on the angle of incidence of the beam ray with respect to the keyhole surface, Bergström (2008). The keyhole surface geometry is governed by both the energy balance between beam, plasma and pool, and the force balance between plasma and pool. The various physical phenomena involved in keyhole laser welding are thus complex and tightly coupled.

The relative order of magnitude of the above physical phenomena can change with the operating laser wavelength: 1 μm and 10 μm wavelengths have distinct impact on beam transport, scattering, attenuation and absorption. The beam

produced at a laser exit uses to be an ideal beam. Its power distribution in a plane perpendicular to the direction of beam propagation varies with the radial and angular position according to the laser TEM mode. The ideal beam may be altered along its transport towards the workpiece. Besides, wavelengths of about 1 μm can be transmitted through flexible fiber glass optics without being absorbed, making them suited to robot applications, contrary to the 10 μm wavelength. Laser light transported in an optic fiber reflects within the fiber, resulting in a beam intensity distribution close to a TEM_{00} mode at the fiber exit, even if the input fiber signal is a higher TEM mode, Kaplan (2011). The laser beam distribution profile significantly affects the keyhole dynamics, and thus the possible formation of defects such as pores, Volpp and Vollerstsen (2015).

Wavelengths of the order of 1 and 10 μm have different abilities to interact with the vaporized metal, the resultant plasma plume and fumes. Due to its wavelength dependence, the iB-absorption mechanism is more important for long than for short wavelength lasers. A 10 μm beam cannot penetrate as deep into dense plasma as a 1 μm beam since the radiation frequency can more easily approach the plasma frequency and facilitate wave damping. At plasma temperatures around 10 kK the iB-absorption starts to decrease with increasing temperature, Katayama (2013). As a result high temperature plasma can have a blocking effect as it prevents the laser energy from reaching the bottom wall of the keyhole, Zhou et al. (2006).

For a given laser power density, the ionization degree of the plasma plume is weaker for 1 μm than for 10 μm laser, implying different temperature distributions in the metal plasma and on the keyhole surface. A comparative study was done by Johnston and Dawson (1973) at 5×10^{10} W/cm^2, so above the power density range used in laser welding. They observed that the maximal electron temperature reaches about 50 eV for a Nd:YAG laser while it exceeds 100 eV for a CO_2 laser. A more recent study by Hassanein et al. (2010) gives similar results. The plasma has an impact on the absorption of the beam energy by the material, since the absorption coefficients increase with temperature, Hoffman and Szymanski (2002), Kaplan (2012). However, it also decreases with the wavelength.

Finally the fume particles produced by 1 and 10 μm laser differ in size distribution (smaller for the latter) and amount. The fumes have thus different impacts on laser power attenuation.

To summarize this introduction, keyhole laser welding is a complex multiphysical problem involving light-matter interaction, conduction, melting, vaporization, plasma generation, fluid flow and surface deformation. The first models developed to improve the physical understanding of keyhole laser welding addressed the beam-matter interaction and heat transfer. The fluid flow was neglected, although convective heat transfer could be included. The advantage of this simplification is to allow performing, under suited assumptions, an analytic resolution of the problem. A review of both analytic and numerical models based on conduction heat transfer was done by Mackwood and Crafer (2005). The more recent generation of models takes into account fluid flow; it implies numerical resolution based on CFD techniques. The aim of this paper is to summarize today's state of the art about the modelling of keyhole laser welding when accounting for fluid flow. This paper is divided into two main sections. The first section addresses the beam-matter interaction. The second part focusses on thermal fluid aspects. The last section concludes with some open questions.

2. Modelling of beam-matter interaction

Laser beams used in welding applications can be described by the electromagnetic theory of optics based on Maxwell equations. Assuming that

- the magnetic field intensity $\vec{H}$ and the electric field $\vec{E}$ are relatively small so that linear optics is valid,
- the optical media is homogeneous, isotropic and non-dispersive (the electric permittivity ε and the magnetic permittivity μ of the media have the same values at all points, do not depend on the direction of propagation, and do not depend on the wave frequency),
- the media is free from charge at the space scale considered (the characteristic space length is larger than the Debye length),

the Maxwell equations can be rearranged to obtain the Helmholtz equation used in physical wave optics. If it is also assumed that

- the media is not conducting,
- the shape of the wave function is a simple harmonic plane wave,

the Maxwell equations further reduce to the wave equation whose solution leads to the Fresnel's laws of geometrical optics. Geometrical optics and physical wave optics are today the two approaches used in combination with thermal fluid flow to model laser keyhole welding. Geometrical optics was already used for determining the keyhole profile before considering the fluid flow. Some of these models are now used combined with fluid flow models. They provide the heat input through the surface of the keyhole cavity and allow setting boundary conditions needed by the thermal fluid equations. Some of these models are thus first recalled (see Mackwood and Crafer (2005) for further details).

The model developed by Kaplan (1994) allows calculating an asymmetric keyhole profile using the point-by-point method at both front wall and back wall of the keyhole. The beam is discretized in a finite number of rays (ray tracing method). The path of each ray inside the keyhole is calculated and the amount of energy absorbed by the surface is expressed as function of wavelength, polarization and angle of incident. The energy balance between the absorbed laser power and the losses due to heat conduction and convection is solved locally. To set the boundary conditions of this heat conduction problem, the heat transfer from the cavity wall to the workpiece is derived from the moving line source introduced by Rosenthal while the keyhole surface temperature is set to the evaporation temperature. The resolution method is an iterative process. The first iteration addresses the direct Fresnel absorption of geometrical optics. The second iteration takes into account multiple Fresnel and iB- absorption. This model is used by Zhang et al. (2011) combined with the fluid flow.

Based on this approach Jüptner et al. (1997) have investigated the influence of scattering in the metal vapour above the keyhole on beam damping. Matsunawa and Semak have developed a model for transient behavior of the front wall of the keyhole; see Matsunawa and Semak (1997) as well as Semak and Matsunawa (1997). They did conclude that convection should not be neglected in the energy balance equation. They did also observe that the cavity front wall may not have a temperature equal or close to the boiling temperature, and it may not move at the same velocity as the laser beam. Solana and Negro (1997) employed both a top-hat and a Gaussian distribution for the laser beam, assuming that the beam rays propagate along straight lines. Fabbro and Chouf (2000) determined the geometry of the keyhole surface at high welding velocity when the cavity front wall is inclined, and did investigate laser beam intensity allowing maintaining wall stability when the wall velocity exceeds the welding velocity. Their approach is also used by Amara and Fabbro (2008) combined with the fluid flow. Jin at al. (2012) did investigate the beam propagation and damping within keyhole geometries set from experimental observations. They assumed that the cavity has a circular section that varies with the depth. This assumption was also used by Xu et al. (2011) and Amara and Fabbro (2008). Besides Jin et al. assumed a Gaussian beam, implying that the beam rays propagate along hyperboloids rather than straight lines. They thus used the Gaussian optic theory rather than the geometrical optic theory to track the beam rays. They observed an uneven distribution of the beam energy on the keyhole surface, and some absorption close to the keyhole mouth that might explain why it remains open. Up to now Gaussian optics does not seem to be used combined with the fluid flow.

Concerning the modelling of beam-matter interaction when accounting for fluid flow, four mains approaches can be found. One is semi-empirical while the three others are derived from electromagnetic theory.

In the simplest case the keyhole physics is decoupled from the convective transport. A semi-empirical source term of heat flux into the cavity wall, which can be used as source term for the fluid equations, is imposed. This approach was used by Chen and Wang (2003), and Cho and Na (2009) with a source term including an adjustable parameter.

The two next approaches are based on geometric ray optics and the ray tracing method. This is the most commonly used method in the field. One of these approaches consists in calculating the keyhole profile decoupled from the convective transport (in the sense decoupled from the resolution of the Navier-Stokes equations). Here too it results in a term of heat flux into the keyhole wall that acts as source term in the fluid equations. But contrary to the previous semi-empirical approach, direct and multiple Fresnel absorptions are accounted for. However the iB-absorption is not always taken into account, even for CO_2 laser (see Table 1, column B-M). Due to the decoupling from the fluid flow, this approach is limited to moderate welding speed for which the bending of the keyhole against the welding speed is not significant.

The next approach extends to high welding speed since it couples the ray tracing method with the resolution of the fluid equations. It was introduced by Ki et al. (2001), and used by several authors, as indicated in table 1 (with the letter c in the column B-M).

The last approach is based on physical wave optics with the Helmholtz equation. Although applied since long in other fields such as the attenuation of radio waves by the atmosphere, its introduction in the field of keyhole laser welding is very recent, see Courtois et al. (2013). In the Helmholtz equation the damping factor is proportional to the electric conductivity of the media. Courtois et al. derived simple wave solutions setting the electric conductivity to zero; in that case the Helmholtz equation reduces to the Eikonal equation. An advantage of this approach is that the shape of the wave function does not need to be assumed a priori. A drawback of the implementation used by these authors is that the size of the mesh elements needs to be smaller than the wavelength of the laser. The authors proposed to circumvent this numerical difficulty changing the wavelength from 1.06 μm to 50 μm and rescaling the results. In this way they could apply the same mesh size to both the electromagnetic problem and the fluid flow problem.

3. Modelling of thermal fluid

Molten and vapour metal flow is of high importance when modeling keyhole laser welding since the keyhole cavity surface is dynamic; the surface deformation may become unstable and cause weld defects such as porosity. Models accounting for both beam-matter interaction and the fluid flow are listed in Table 1. The references are in chronological order according to publication date. Most of these thermal fluid models assume:

- Newtonian and laminar fluids in a fixed reference frame,
- Constant thermodynamic and transport properties,
- At least two phases (liquid and solid),
- Solidification and melting (mushy zone model),
- Vaporization,
- Surface deformation.

The fluid model is thus generally made of a continuity equation expressed here in a fixed reference frame

$$\partial_t \rho + \nabla \cdot (\rho \vec{u}) = S_\rho \tag{1}$$

where ρ denotes the density of the mixture, t the time and $\vec{u}$ the velocity. S_ρ is a source term of mass production by vaporization. As expected this term is set to zero in all the two-phase (solid/liquid) models. Probably for simplicity, S_ρ is also set to zero in most of the models accounting for the flow of the vapour phase. A non-zero source term S_ρ is modeled by Courtois et al. (2013) as indicated in table 1 (with the letter S_ρ in the column *V*). In the general case the density depends on both pressure and temperature. In most models both dependencies are ignored.

The Navier-Stokes equation can write

$$\begin{aligned}\partial_t(\rho\vec{u}) + \nabla \cdot (\rho\vec{u}\otimes\vec{u}) = \nabla \cdot \left[-pI + \mu\left((\nabla\vec{u}) + (\nabla\vec{u})^T\right)\right] + \rho\vec{g} - \alpha_l\,\rho_l\,\beta_l\,(T - T_{melt})\vec{g} \\ + K_D\vec{u} - \left[\sigma\vec{n}_s\kappa - \nabla_s T\,\frac{\partial\sigma}{\partial T}\right]\delta(\alpha_l)\end{aligned} \tag{2}$$

where p is the pressure, I the identity matrix, μ the viscosity of the liquid, $\vec{g}$ the gravitational acceleration. α_l, ρ_l and β_l are the volume fraction, the density and the volume expansion coefficient of liquid, respectively. K is a coefficient of frictional dissipation in the mushy zone (usually according to Carman-Kozeni equation), σ is the surface tension, $\vec{n}_s$ and κ the normal vector and the curvature of the liquid/vapour interface, and δ is the Dirac function. The last term on the first line of Eq. (2) is the buoyancy force; this force is often neglected as indicated in Table 1. The second term in the second line is the capillary force, and the last term is the Marangoni (or thermocapillary) force induced by temperature gradients of surface tension. The capillary force is a leading order force governing the shape of the liquid/vapour interface on the top of the melt pool. For metals used in welding it depends on both temperature and

element concentrations in the metal, more specifically surfactants, Al-Kazzaz et al. (2008). However it is often assumed constant in the models (see Table 1), may be due to the lack experimental data for the surface tension of liquid metals at high temperature.

The recoil pressure is considered to be a driving force for fluid flow in the keyhole cavity. It keeps the keyhole open while the surface tension and gravitational forces try to close it. When the source term of vapour production is modeled in Eq. (1) the recoil pressure is automatically included in the pressure p of Eq. (2). When on the contrary S_ρ is set to zero the recoil pressure force needs to be added to Eq. (2) in the form of a boundary condition to model surface deformation, as done by most authors and indicated in table 1 (with the letter p_r in the column *V*). When surface deformation is not described, all the surface forces (surface tension, Marangoni force and recoil pressure) are ignored in the Navier-Stokes equations, and suited boundary conditions are set to prevent the surface from moving, as done by Mościcki et al. (2006), Rai et al. (2007), and Zhang et al. (2011).

When modeling surface deformation, the numerical evaluation of the surface forces (surface tension, Marangoni, possibly recoil pressure) requires calculating geometrical properties (normal and curvature) of the liquid/vapour interface. There exist different approaches for mathematically modeling a free surface, such as interface tracking and interface capturing. The former is demanding in terms of computational resources since it treats the free surface as a sharp interface and follows its motion. This approach does not seem to be used for keyhole laser welding simulation. The interface capturing approach is less accurate and less demanding in computational resources since it converts the problem to the resolution of a partial differential equation, allowing calculating complex interfaces. Level Set (LS) and Volume of Fluid (VOF) methods are the two families of interface capturing methods used in this field. The level set method is the most accurate but in its original version it does not satisfy mass conservation. The VOF method satisfies mass conservation but in its original version it is quite diffusive. Several improved versions exist such as the narrow band LS used by Ki et al. (2002), the Sharper Surface Force VOF used by Otto et al. (2011), as well as hybrid versions.

For a mixture the energy equation may be easier to formulate with the temperature, although some authors do prefer the mixture enthalpy,

$$\partial_t\left(\rho C_p T\right) + \nabla\cdot\left(\rho C_p T\vec{u}\right) = \nabla\cdot(\lambda\nabla T) + Q_{laser} + Q_{vap} \tag{3}$$

C_p denotes the specific heat for the mixture, T the temperature, λ the thermal conductivity of the mixture. The mixture properties are derived from the properties of the components doing a mass average or a volume average calculation, depending on the property. A special treatment (smoothing) is usually needed at the liquid/vapour interface across which the properties may vary by several orders of magnitude. The thermodynamic and transport properties of the components depend on temperature T and composition, and possibly on pressure p for the metal vapour. However most of the models of Table 1 (not Amara and Fabbro (2008)) assume thermodynamic and transport properties independent of p and T. Q_{laser} is the laser beam energy source term (discussed in section 2). For the models based on the ray tracing method it models the energy absorbed by direct and multiple Fresnel absorption, and in some cases it accounts for the damping through iB-absorption (see column B-M in Table 1). Q_{vap} is the latent heat of vaporization.

The system of fluid equations (1)-(3) applies in regions with a Knudsen number large enough. When vaporization takes place and the saturation pressure is large compared to the ambient pressure, a vapour layer with a thickness of some mean free paths (called Knudsen layer) develops at the vapour/liquid interface. In this layer the Knudsen number is smaller than unity, and thermodynamic equilibrium is not satisfied so that kinetic theory should be used rather than the continuum approach. A simple alternative consists in applying across the Knudsen layer the jump relations on pressure, temperature and density proposed by Knight (1979). The models taking into account the Knudsen layer through Knight's jump relations are indicated in Table 1 (with a cross in column K).

Table 1 shows the diversity in models used for simulating keyhole laser welding when accounting for the fluid flow. Because of lack of space this indication is only partial. Consider for instance vaporization. Most of the models account for vaporization through the recoil pressure (indicated with p_r in the column V of Table 1). However they do it based on different formulations with different temperature dependence. As an illustration Ki et al. (2002), and Dasgupta et al. (2007) use the recoil pressure proposed by Ytrehus and Østmo (1996), while Lee et al. (2002) and Cho and Na (2006) use the Clausius-Clapeyron model. Zhou and Tsai (2006), (2008), and Amara and Fabbro (2008) use the model developed by Semak and Matsunawa (1997), while Geiger et al. (2009) and Koch et al. (2010) use a fourth

Table 1. Categorization of models with both beam-mater interaction and thermal fluid flow

Author	Domain of study	Main properties of model								Some other properties
		D	B-M	S	V	H	M	B	K	
Ki et al. (2001), (2002)	cw CO_2 laser, steel	2	*cF*	*L*	p_r, h_{fg}	×	×		×	1st model Narrow band LS
Lee et al. (2002)	mild steel	2	*cF*	*V*	h_{fg}		×	×	×	Assume sonic flow in Knudsen layer
Chen and Wang Wang and Chen (2003)	cw CO_2 laser, iron	3*	*FB**							*Cylindrical keyhole cavity Only gas flow; no thermal aspect
Cho et al. (2006)	pulsed Nd:YAG S304 steel	3	*cF*	*V*	p_r, h_{fg}					Constant surface tension Radiative cooling cavity-room
Zhou et al. (2006)	pulsed Nd:YAG	2	*cFB*	*V*	p_r, h_{fg}		×	×	×	Vapour included (absorbing-emitting media; no flow)
Mościcki et al. (2006)	CO_2 laser, Ar, He shielding gas	3	*B*							Mixture of gas and metal vapour
Dasgupta et al. (2007)	cw CO_2 laser, galvanized steel	3	*cF*	*L*	p_r, h_{fg}	×	×		×	Adaptive mesh refinement, Narrow band Level Set
Rai et al. (2007)	Stainless steel, Al alloy	3			h_{fg}	×		×		No surface deformation Constant "Fresnel" absorption
Amara & Fabbro (2008)	cw Nd:YAG, Fe	3	*F**	*V*	p_r, h_{fg}		×	×	×	* with model of Fabbro and Chouf (2000)
Zhou & Tsai (2008)	Hybrid laser-MIG 304 Stainless steel	2	*cFB*	*V*	p_r, h_{fg}		×	×	×	Vapour flow included, Compressible vapour
Gao et al. (2009)	Al alloy	2	*	*V*	p_r, h_{fg}		×	×		*Gaussian with adjustable parameter
Geiger et al. (2009)	Nd:YAG	3	*cF*	*V*	p_r, h_{fg}	×				Sharper Surface Force VOF
Koch et al. (2010)	CO_2 and Yb:YAG	3	*cF*	*V*	p_r, h_{fg}	×				Sharper Surface Force VOF
Cho et al. (2010)	CO_2 laser-GMA Carbon steel SS400	3	*c*F*	*V*	p_r, h_{fg}	×		×		*simplified Fresnel model
Pang et al. (2011)	cw Nd:YAG, Al alloy	3	*cF*	*L*	p_r, h_{fg}	×	×	×	×	Constant surface tension, Vapour phase included
Otto et al. (2011)	Stainless steel	3	*cF*	*V*	p_r, h_{fg}	×	×			Sharper Surface Force VOF, vapour flow included
Zhang et al. (2011)	Ti-6Al-4V	3	*FB**	*V*	h_{fg}		×	×		Vapour and gas flow included *with model of Kaplan (1994)
Cho et al. (2012)	fibre laser, carbon steel	3	*cF**	*V*	p_r, h_{fg}	×	×	×		Vapour flow included *with diffraction
Otto et al. (2012)		3	*cF*	*V*	p_r, h_{fg}	×				Sharper Surface Force VOF, vapour flow included
Tan et al. (2013)	Pulsed, 304 Stainless steel	3	*cFB**	*L*	p_r, h_{fg}		×	×	×	Vapour flow included *with Beer's law
Courtois et al. (2013)	Nd:YAG, DP600 steel	2	*cF**	*L*	S_ρ, h_{fg}			×	×	*Eikonal equation Vapour flow included

D – *number of space dimensions,* **B-M** – *beam-matter interaction with beam and flow coupled (c), multiple Fresnel absorption (F), iB-absorption (B),* **S** – *surface deformation using Level Set (L) or VOF (V),* **V** – *vaporization modeled through: mass source (S_ρ), recoil pressure (p_r), latent heat of vaporization (h_{fg}),* **H** –*heat source in relative motion with the base metal (if ×),* **M** –*Marangoni force modelled (if ×),* **B** –*buoyancy modelled (if ×),* **K** –*Knudsen layer modelled (if ×).*

model (see Dowden (2009)).

Some models consider radiative cooling, others do not. Radiative cooling of the keyhole cavity surface is modeled with the grey body model (originally developed for a small surface surrounded by a media that does not interact with the radiation, and enclosed in a much larger surface at some reference temperature). In Cho and Na (2006), Lee et al. (2002), Zhou and Tsai (2008), Pang et al. (2011), and Cho et al. (2012), the reference cooling temperature is supposed to be the room temperature. Similar in Rai et al. (2007) but in that later case there is no cavity surface since surface deformation is not taken into account. In Zhou et al. (2006) the reference cooling temperature is the temperature of the metal vapour (the plasma temperature).

The thermodynamic and transport properties are known to depend weakly on pressure and strongly on temperature. However the temperature dependence of both liquid and vapour phases is often neglected. In some cases it is also assumed that solid and liquid metal phases have the same thermodynamic properties, as in Lee et al. (2002), Cho and Na (2006), Roy et al. (2006), Rai et al. (2007), Amara and Fabbro (2008), Geiger et al. (2009), Koch et al. (2010), Pang et al. (2011), and Otto et al. (2011), (2012).

The simulation models listed in Table 1 did allow gaining a deeper understanding of the keyhole laser welding process. Some of these results are now summarized. Ki et al. (2002) did comparative studies activating one by one elements of their model. Their numerical calculations show a dramatic change in both liquid and vapour flow field when activating evaporation. The deformation of the liquid/vapour surface has a substantial influence on liquid flow in the pool. Fresnel multiple reflection leads to a larger keyhole cavity (broader and deeper). It has also a substantial influence on the vapour flow and results in a larger plume, and a drastic rise of temperature at the cavity surface. Finally the beam intensity profile deviates from the original Gaussian.

Lee et al. (2002) studied the formation and stability of the keyhole cavity. Their simulation results show both upward and downward flow along the wall of the keyhole cavity. These flows are generated by the recoil pressure and the surface tension, respectively. As they met a protrusion forms, and grows until it closes the cavity, resulting in cavity collapse and void trapping. The keyhole cavity is thus unstable, even in stationary conditions. They also observed that the Marangoni force does not have any significant effect on the upward liquid flow within the cavity, although it promotes outward flow of the melt at the keyhole entrance.

Zhou and Tsai (2006) modelled a pulsed Nd:YAG laser and stainless steel with sulfur to study the keyhole formation and evolution in time up to its collapse during a pulse. They observed that as the metal vapour forms into the keyhole cavity, plasma radiation promotes metal vaporization and deeper drilling of the cavity. The iB-absorption, and thus the plasma temperature, as well as multiple Fresnel reflection increase while the temperature gradient along the cavity surface decreases, resulting in a broadening of the molten pool. Along the drilling process increasing surface tension and hydrostatic force oppose the recoil pressure, thus weakening the drilling process. On the top of the pool the Marangoni force pushes the liquid metal outwards from the cavity opening. At some distance from the cavity opening (on the top surface) the temperature gradient decreases and eventually reaches an inflection point (due to the presence of sulfur in the steel) leading to an inversion of the surface flow direction. On the top of the keyhole cavity wall hydrostatic force and surface tension push the liquid metal downwards while on the bottom the recoil pressure pushes it upwards. The combination of these opposed forces results in a clockwise vortex at the keyhole shoulder, and causes a broadening of the heat affected zone. Finally at the end of the pulse the keyhole force balance changes due to the rapid temperature decrease, vaporization vanishes, and a downward flow closes the upper part of the cavity. Then porosity may form depending on the relative speed of the downward flow and solidification.

Amara and Fabbro (2008) showed with their model that the oscillations observed at the surface of the pool could be suppressed by using a side gas jet.

Tan et al. (2013) observed with their model that even though Nd:YAG is less sensitive to iB-absorption than a CO_2 laser, the attenuation of a Nd:YAG laser power can reach up to 22% of the total power.

4. Conclusion

Several models combining beam-matter interaction and fluid flow to study keyhole laser welding have been developed during the past 15 years, since the first model by Ki et al. (2001). Hopefully most of these models should be represented in this review. The variety of these models and some of the simplifications discussed in the previous

sections show that this field is still under development. For instance the influence of the temperature dependence of the material properties has been little investigated. The thermodynamic properties of the most common solid metals used in welding are in many cases well know. However thermodynamic and transport properties (as well as surface tension) of these metals in liquid phase are documented over a rather narrow range of (low) temperature that does not cover the complete liquid temperature range. The metal plasma is modelled as a gas in the fluid models, not yet as a plasma (thus a conducting media); the consequence of this simplification is not yet known. The influence on the fluid flow of the shape of the laser light wave function, of the beam rays propagation (e.g. along hyperboloids rather than straight lines) is not yet known too. Little attention has been given to the difficult problem of fumes modelling, Mie-scattering and Rayleigh scattering. But the main issue may be the need for experimental data allowing further validating the models. Experimental observation is indeed another challenge due to the high temperatures in the weld and especially in the keyhole, as well as the difficult access to the metal vapour inside the cavity.

Acknowledgements

This work was supported by VINNOVA, programme NFFP, project no. 2013-01139, in collaboration with GKN. These supports are gratefully acknowledged.

References

Al-Kazzaz, H., Medraj, M., Cao, X., Jahazi, M., 2008. Nd:YAG laser welding of aerospace grade ZE41A magnesium alloy: modelling and experimental investigations. Materials Chemistry and Physics **109**(1), 61-76.

Amara, E.H., Fabbro, R., 2008. Modelling of gas jet effects on the melt pool movements during deep penetration laser welding. Journal of Physics D: Applied Physics **41**(5), 055503.

Bergström, D., 2008. The absorption of laser light by rough metal surfaces. PhD Thesis, Luleå University of Technology, Sweden

Chen, X., Wang, H.X., 2003. Three-dimensional modeling of the laser-induced plasma plume characteristics in laser welding. Journal of Physics D: Applied Physics **36**(6), 628-639.

Chen, X., Wang, H.X., 2003. Prediction of the laser-induced plasma characteristics in laser welding: a new modelling approach including a simplified keyhole model. Journal of Physics D: Applied Physics **36**(13), 1634-1643.

Cho, J.H., Na, S.J., 2006. Implementation of real-time multiple reflection and Fresnel absorption of laser beam in keyhole. Journal of Physics D: Applied Physics **39**(24), 5372-5378.

Cho, J.H., Na, S.J., 2009. Three-dimensional analysis of molten pool in GMA-laser hybrid welding. Welding Journal **88**, 35s-43s.

Cho, W.I., Na, S.J., Chi, M.H., Lee, J.S., 2010. Numerical study of alloying element distribution in CO_2-laser GMA hybrid welding. Computational Materials Science **49**(4), 792-800.

Cho, W.I., Na, S.J., Thomy, C., Vollertsen, F., 2012. Numerical simulation of molten pool dynamics in high power disk laser welding. Journal of Materials Processing Technology **212**(1), 262-275.

Courtois, M., Carin, M., Le Masson, P., Gaied, S., Balabane, M., 2013. A new approach to compute multi-reflections of laser beam in a keyhole for heat transfer and fluid flow modelling in laser welding. Journal of Physics D: Applied Physics **46**(50), 505305.

Dasgupta, A.K., Mazumder, J., Li, P., 2007. Physics of zinc vaporization and plasma absorption during CO_2 laser welding. Journal of Applied Physics **102**, 053108.

Dowden J.M. (Ed.), 2009. The theory of laser material processing, Heat and Mass Transfer in Modern Technology, Springer Series in Material Science.

Fabbro, R., Chouf, K., 2000. Keyhole modeling during laser welding. Journal of Applied Physics **87**, 4075-4083.

Gao, Z., Wu, Y., Huang, J., 2009. Analysis of weld pool dynamic during stationary laser-MIG hybrid welding. Int. Journal of Advanced Manufacturing Technology **44**(9-10), 870-879.

Geiger, M., Leitz, K.H., Koch, H., Otto, A., 2009. A 3D transient model of keyhole and melt pool dynamics in laser beam welding applied to the joining of zinc coated sheets. Production Engineering Research and Development **3**, p. 127-136.

Hassanein, A., Sizyuk, V., Harilal, S.S., Sizyuk, T., 2010. Analysis, simulation and experimental studies of YAG and CO_2 laser produced plasma for EUV lithography sources. Proceedings of SPIE 7636, The International Society for Optical Engineering, 76360A.

Hoffman, J., Szymanski, Z., 2002. Absorption of the laser beam during welding with CO_2 laser. Optica Applicata **32**(1-2), 129-146.

Jin, X., Cheng, Y., Zeng, L., Zou, Y., Zhang, H., 2012. Multiple reflections and Fresnel absorption of Gaussian laser beam in an actual 3D keyhole during deep penetration laser welding. International Journal of Optics 2012, 361818.

Johnston, T. W., Dawson, J. M., 1973. Correct values for high frequency power absorption by inverse bremsstrahlung in plasmas. Physics of Fluids **16**, 722.

Jüptner, W., Franz, Th., Sikau, J., Sepold, G., 1997. Laser interaction with plasma during material processing. Laser Physics **7**(1), 202-207.

Kaplan, A., 1994. A model of deep penetration laser welding based on calculation of the keyhole profile. Journal of Physics D: Applied Physics **27**(9), 1805-1814.

Kaplan, A., 2011. Influence of the beam profile formulation when modeling fiber-guided laser welding. Journal of Laser Applications **23**, 042005.

Kaplan, A., 2012. Absorptivity modulation on wavy molten steel surface: the influence of laser wave-length and angle of incidence. Applied Physics Letters **101**, 151606.

Kaplan, A., 2012. Fresnel absorption of 1μm- and 10μm-laser beams at the keyhole wall during laser beam welding: Comparison between smooth and wavy surfaces. Applied Surface Science **258**(8), 3354-3363.

Katayama, S. (Ed.), 2013, Handbook of Laser Welding Technologies, Elsevier.

Ki, H., Mohanty, P.S., Mazumder, J., 2001. Modeling of high density laser material interaction using fast level set method. Journal of Physics D: Applied Physics **34**(3), 364-372.

Ki, H., Mohanty, P.S., Mazumder, J., 2002. Modeling of laser keyhole welding: Part I. Mathematical modeling, numerical methodology, role of recoil pressure, multiple reflections, and free surface evolution. Metallurgical and Materials Transactions A **33A**, 1817-1830.

Ki, H., Mohanty, P.S., Mazumder, J., 2002. Modeling of laser keyhole welding: Part II. Simulation of Keyhole Evolution, Velocity, Temperature Profile and Experimental Verification. Metallurgical and Materials Transactions A **33A**, 1831-1842.

Knight, C.J., 1979. Theoretical modeling of rapid surface vaporization with back pressure. AIAA Journal **17**(5), 519-523.

Koch, H., Leitz, K.H., Otto, A., Schmidt, M., 2010. Laser deep penetration welding simulation based on a wavelength dependent absorption model. Physics Procedia **5**(B), 309-315.

Lee, J.Y., Ko, S.H., Farson, D.F., Yoo, C.D., 2002. Mechanism of keyhole formation and stability in stationary laser welding. Journal of Physics D: Applied Physics **35**, 1570-1576.

Mackwood, A.P., Crafer, R.C., 2005. Thermal modelling of laser welding and related processes: a literature review. Optics and Laser Technology **37**(2), 99-115.

Matsunawa, A., Semak, V., 1997. The simulation of front keyhole wall dynamics during laser welding. Journal of Physics D: Applied Physics **30**(5), 798-809.

Mościcki, T., Hoffman, J., Szymański, Z., 2006. Modelling of plasma plume induced during laser welding. Journal of Physics D: Applied Physics **39**, 685-692.

Otto, A., Koch, H., Leitz, K.H., Schmidt, M., 2011. Numerical simulations – a versatile approach for better understanding dynamics in laser material processing. Physics Procedia **12**(A), 11-20.

Otto, A., Koch, H., Vazquez, R.G., 2012. Multiphysical simulation of laser material processing. Physics Procedia 39, 843-852.

Pang, S., Chen, L., Zhou, J., Yin, Y., Chen, T., 2011. A three-dimensional sharp interface model for self-consistent keyhole and weld pool dynamics in deep penetration laser welding. Journal of Physics D: Applied Physics **44**, 025301.

Rai, R., Elmer, J.W., Palmer, T.A., DebRoy, T., 2007. Heat transfer and fluid flow during keyhole mode laser welding of tantalum, Ti-6Al-4V, 304L stainless steel and vanadium. Journal of Physics D: Applied Physics **40**, 5753-5766.

Rai, R., Roy, G.G., DebRoy, T., 2007. A computationally efficient model of convective heat transfer and solidification characteristics during keyhole mode laser welding. Journal of Applied Physics **101**, 054909.

Roy, G.G., Elmer, J.W., DebRoy, T., 2006. Mathematical modeling of heat transfer, fluid flow, and solidification during linear welding with pulsed laser beam. Journal of Applied Physics **100**, 034903.

Semak, V., Matsunawa, A., 1997. The role of recoil pressure energy balance during laser materials processing. Journal of Physics D: Applied Physics **30**(18), 2541-2552.

Solana, P., Negro, G., 1997. A study of the effect of multiple reflections on the shape of the keyhole in laser processing of materials. Journal of Physics D: Applied Physics **30**(23), 3216-3222.

Tan, W., Bailey, N.S., Shin, Y.C., 2013. Investigation of keyhole plume and molten pool based on a three-dimensional dynamic model with sharp interface formulation. Journal of Physics D: Applied Physics **46**(5), 055501.

Volpp, J., Vollertsen, F., 2015. Modeling keyhole oscillations during laser deep penetration welding at different spatial laser intensity distributions, Production Engineering Research and Development **9**, 167-178.

Wang H-X., Chen, X., 2003. Three-dimensional modelling of the laser induced plasma plume characteristics in laser welding. Journal of Physics D: Applied Physics **36**(6), 628-639.

Xu, G.X., Wu, C.S., Qin, G.L., Wang, X.Y., Lin, S.Y., 2011. Adaptive volumetric heat source models for laser beam and laser + pulsed GMAW hybrid welding processes. Int. Journal of Advanced Manufacturing Technology **57**, 245-255.

Ytrehus, T., Østmo, S., 1996. Kinetic theory approach to interphase processes, International Journal of Multiphase Flow **22**(1), 133-155.

Zhang, L., Zhang, J., Zhang, G., Bo, W., Gong, S., 2011. An investigation on the effects of side assisting gas flow and metallic vapour jet on the stability of keyhole and molten pool during laser full-penetration welding. Journal of Physics D: Applied Physics **44**(13), 135201.

Zhou, J., Tsai, H.L., Wang, P.C., 2006. Transport Phenomena and Keyhole Dynamics during Pulsed Laser Welding. Journal of Heat Transfer **128**(7), 680-690.

Zhou, J., Tsai, H.L., 2008. Modeling of transport phenomena in hybrid laser-MIG keyhole welding. International Journal of Heat and Mass Transfer **51**(17-18), 4353-4366.